

# RSC Advances



This is an *Accepted Manuscript*, which has been through the Royal Society of Chemistry peer review process and has been accepted for publication.

*Accepted Manuscripts* are published online shortly after acceptance, before technical editing, formatting and proof reading. Using this free service, authors can make their results available to the community, in citable form, before we publish the edited article. This *Accepted Manuscript* will be replaced by the edited, formatted and paginated article as soon as this is available.

You can find more information about *Accepted Manuscripts* in the [Information for Authors](#).

Please note that technical editing may introduce minor changes to the text and/or graphics, which may alter content. The journal's standard [Terms & Conditions](#) and the [Ethical guidelines](#) still apply. In no event shall the Royal Society of Chemistry be held responsible for any errors or omissions in this *Accepted Manuscript* or any consequences arising from the use of any information it contains.

# Enhanced Electrochemical Performance of $\text{LiMn}_2\text{O}_4$ Cathode with a $\text{Li}_{0.34}\text{La}_{0.51}\text{TiO}_3$ -Coated Layer

Sijiang Hu<sup>a,c</sup>, Yu Li<sup>b</sup>, Feiyan Lai<sup>b</sup>, Xiaohui Zhang<sup>b</sup>, Qingyu Li<sup>b</sup>, Youguo Huang<sup>b</sup>, Ximing Yuan<sup>a,\*</sup>, Jianjun Chen<sup>d</sup>, Hongqiang Wang<sup>b,c,\*</sup>

<sup>a</sup>School of Materials Science and Chemistry, China University of Geosciences, Wuhan 430074, PR China

<sup>b</sup>Guangxi Key Laboratory of Low Carbon Energy Materials, School of Chemistry and Pharmaceutical Sciences, Guangxi Normal University, Guilin 541004, PR China

<sup>c</sup>Hubei Key Laboratory for Processing and Application of Catalytic Materials, College of Chemical Engineering, Huanggang Normal University, Huanggang 438000, PR China

<sup>d</sup>Research Institute of Tsinghua University in Shenzhen, Shenzhen 518057, P.R. China

Corresponding author's information:

Email address: whq74@mailbox.gxnu.edu.cn (H Wang), xmyuan@foxmail.com (X. Yuan)

Fax number:+86 773 5854077

## Abstract

Spinel cathode materials consisting of  $\text{LiMn}_2\text{O}_4@ \text{Li}_{0.34}\text{La}_{0.51}\text{TiO}_3$  (LMO@LLTO) have been synthesized by a new and facile solid-phase route in air. When used as cathode of lithium ion battery, the LLT01( $\text{LiMn}_2\text{O}_4$  with 20 nm  $\text{Li}_{0.34}\text{La}_{0.51}\text{TiO}_3$  coating) sample tested at 1 C rate exhibits 9.2% capacity loss and 90.4% capacity retention after 200 cycles at 25 °C and 55 °C, respectively. The improved cycling performance of composites is attributed to the LLT01 coating on the surface of spinel particles. The polycrystalline LLTO-coated layer could provide superior ionic conductivity and prevent Mn dissolution in electrolyte during electrochemical cycling.

**Keywords:** cathode; surface coating; solid electrolyte; lithium ion battery

## 1. Introduction

Recently, the lithium ion batteries (LIBs) are competitive power sources for hybrid electric vehicles (HEVs) and electric vehicles (EVs).<sup>1-3</sup> Many studies on LIBs have been attempted to develop a cathode material with non-toxicity, better safety, longer

life, lower cost, high power density and excellent thermal stability.<sup>4-6</sup> As one of the most promising candidates, spinel  $\text{LiMn}_2\text{O}_4$  material has attracted much attention due to its lower cost and toxicity relative to  $\text{LiCoO}_2$  cathode material, and its fairly high discharge voltage plateau (4.1 V) compared with the working potential of  $\text{LiFePO}_4$  at 3.45 V. The higher working potential leads to the increase of energy density. Moreover, the cells based on  $\text{LiMn}_2\text{O}_4$  have a higher volumetric energy density over its counterparts.<sup>7-12</sup> Unfortunately, the material suffers rapid capacity fading at high temperature, owing to Jahn-Teller effect<sup>13-15</sup> and dissolution of Mn in electrolyte during cycling.<sup>16, 17</sup>

To overcome these obstacles, two kinds of effective strategies have been intensively employed. One way is partially element doping in  $\text{LiMn}_2\text{O}_4$ .<sup>18-21</sup> Reddy et al.<sup>18</sup> reported a series of Co and Cr doped  $\text{LiMn}_2\text{O}_4$  cathode which showed significantly improved cycling performance and excellent rate capability. The other method is surface modification, which provides a shield of the  $\text{LiMn}_2\text{O}_4$ . For example, Lee et al.<sup>7</sup> have shown a novel heterostructure  $\text{LiMn}_2\text{O}_4$  with epitaxially grown layered surface phase, gave a discharge capacity of  $123 \text{ mAh g}^{-1}$  and retained 85% of its initial capacity at  $60^\circ\text{C}$  after 100 cycles.

In addition, various inorganic materials such as  $\text{Al}_2\text{O}_3$ <sup>22, 23</sup>,  $\text{MgO}$ <sup>24, 25</sup>,  $\text{ZrO}_2$ <sup>26, 27</sup>,  $\text{ZnO}$ <sup>28, 29</sup>,  $\text{La}_2\text{O}_3$ <sup>30, 31</sup>,  $\text{NiO}$ <sup>32</sup>,  $\text{CeO}_2$ <sup>33</sup>,  $\text{Mn}_2\text{O}_3$ <sup>34</sup>,  $\text{V}_2\text{O}_5$ <sup>35</sup>, carbon<sup>36</sup>,  $\text{FeF}_3$ <sup>37</sup>,  $\text{AlPO}_4$ <sup>38</sup>, have been widely used as surface modification materials for  $\text{LiMn}_2\text{O}_4$  cathode, which demonstrated obviously improved capacity retention rate, as a result of the protecting for  $\text{LiMn}_2\text{O}_4$  particles from the attack of HF.<sup>39</sup> However, metal oxide coating material

has poor electronic conductivity and low  $\text{Li}^+$  diffusion rate which lead to degradation of electrochemical performance of spinel  $\text{LiMn}_2\text{O}_4$ . Therefore, it is important to develop a high electronic and ionic conductivity surface modification materials.<sup>40</sup> Solid electrolyte  $\text{Li}_{3x}\text{La}_{2/3-x}\text{TiO}_3$  (LLTO) is one of the most promising coating materials, due to its good thermal stability and high ionic conductivity (For crystalline LLTO, the bulk part as high as  $10^{-3} \text{ S cm}^{-1}$  at room temperature).<sup>41</sup> The LLTO layer has a greater enhanced surface intercalation reaction of lithium ions, reduced charge transfer resistance and contact between active electrode materials and electrolyte solution.<sup>42</sup> Besides, the rate capability can be improved by the surface coated layer.

In this work, a facile and efficient route for the preparation of core-shell LMO@LLTO cathode materials is demonstrated. Different from previously reported methods,<sup>[43,44]</sup> the surface coating of LLTO herein is achieved by a two-step synthesis strategy: first liquid-phase coating and second heat treatment. The LLTO coating samples synthesized by usual way was an amorphous phase. The approach adopted in this work is based on a crystalline phase LLTO synthesizing, a solid mixing with  $\text{LiMn}_2\text{O}_4$  and subsequently solid state reaction. We hope the crystalline LLTO benefit to improve lithium ionic conductivity of the interface between cathode material and electrolyte. Significantly, the capacity retention of the cathodes was greatly improved during cycling at high rate and even with operation at  $55^\circ\text{C}$ .

## 2. Experimental

### 2.1. Synthesis

$\text{LiMn}_2\text{O}_4$  were obtained from CITIC Dameng Mining Industries Ltd. The LLTO

powder were prepared by the method reported before.<sup>41</sup> For synthesis of LMO@LLTO samples, LLTO and  $\text{LiMn}_2\text{O}_4$  powder were added into 2-propanol and Tween-20, followed by mixing processes (ultrasonic treatment for 2 h and ball milling for 6 h). The amount of LLTO in the solution was set at mass ratios of LLTO/ $\text{LiMn}_2\text{O}_4$ =1 wt%, 3 wt% and 5 wt% and the corresponding samples were marked as LLT01, LLT03, LLT05 respectively as well as the sample without LLTO marked as LLT0. The obtained gel precursor was dried at 100 °C for 24 h, and then calcined at 500 °C for 4 h in air to form the LLTO layer.

## 2.2. Physical characterization

The crystal structures of the pristine LMO and LMO@LLTO were examined with powder X-ray diffractometer (XRD) on a D/Max-2500 V/PC powder diffractometer equipped with Cu K $\alpha$  radiation ( $\lambda = 1.5406 \text{ \AA}$ ) (Rigaku, Tokyo, Japan). The scanning rate was 3°/min and the scanning range of diffraction angle was  $10^\circ \leq 2\theta \leq 90^\circ$ . The X-ray photoelectron spectroscopy (XPS) was carried out by ESCALAB 250Xi (Thermo) using Al K $\alpha$  radiation (1486.6 eV). The binding energies were calibrated with reference to the C1s spectrum at 284.6 eV. Particle size distribution were performed with a LS-POP (VI) laser particle size analyzer (OMEC, Zhuhai, China). The LLTO coating thickness was observed by transmission electron microscopy (TEM: JEM-2010, JEOL). The morphological features of before and after the coating process was observed with a scanning electron microscope (SEM: Philips, FEI Quanta 200 FEG). Energy-dispersive spectroscopy (EDS) was obtained in conjunction with SEM to determine the element content of powders together with SEM in large field of

view. Electronic conductivity of the samples was measured by the Four-Probe method using a contact-type conductivity meter (Guangzhou Four-Probe Technology Co. Ltd., China). The samples were prepared as follows: the samples were dried at 100 °C for 4 h in a vacuum oven. Then the dried samples were pressed under 20 MPa for 3 min to form a wafer with 12 mm in diameter. The molar ratio of metals (La, Li and Ti) in the samples and contents of Mn dissolved in electrolyte were obtained by inductively coupled plasmaatomic emission spectrometry (ICP-AES, IRIS Intrepid II XSP, Thermo Electron Corporation).

### 2.3. Electrochemical measurements

The electrochemical measurements were carried out on CR2025 coin-type cells using LAND CT2001A tester at 25 °C and 55 °C. For fabrication of the positive electrode, the 90 wt% active material (LLT0, LLT01, LLT03, LLT05) were mixed with acetylene black (5 wt%) and polyvinylidene fluoride (5 wt%) dissolved in N-methylpyrrolidinone onto an Al foil and dried in a vacuum at 80 °C over for 24 h. As formed electrodes were then pressed at a pressure of 2 MPa and further dried at 80 °C for 12 h. Finally, they were cut into wafers with 1.2 cm diameter. The active material mass loading weight was approximately 3.5 mg per wafer. These cathodes were incorporated into cells with a Pure lithium foil anode, a 1 M LiPF<sub>6</sub> electrolyte in a 1:1:1 EC: DMC: DEC solvent (Beijing Institute of Chemical Reagents, China) and a thin polypropylene film used as the separator. The assembly of the 2025 type coin cells was carried out in an Ar-filled glove box with the content of H<sub>2</sub>O and O<sub>2</sub> less than 1 ppm. The cell consists of Al current collector, two electrodes, the anode and

cathode, separated by an electrolyte. Solid electrodes separated by a liquid electrolyte are kept apart by an electrolyte-permeable separator. Galvanostatic charge and discharge measurements were carried out in the voltage range between 3.0 and 4.3 V at different C rates ( $1\text{ C} = 148\text{ mA g}^{-1}$ ). The cyclic voltammograms (CV) and electrochemical impedance spectroscopy (EIS) data were performed using a Zahner IM6 electrochemical workstation (Zahner-Elektrik GmbH & Co. KG, Germany). CV was made at a scan rate of  $0.1\text{ mV s}^{-1}$  in the range 3.0 - 4.3 V at room temperature. And EIS was examined at different cycles by applying an AC voltage of 5 mV over the frequency range of 0.01 Hz to 100 kHz.

### 3. Results and discussion

The XRD patterns of pristine LLTO and LMO@LLTO are shown in Fig. 1. As shown in Fig. 1a, all of these peaks confirmed that the material belongs to the typical single-phase perovskite LLTO (JCPDS card no. 46-0466), with porous network structure in Fig. S1, Electronic Supplementary Information (ESI). The peaks in Fig. 1b can be indexed to cubic  $\text{LiMn}_2\text{O}_4$  spinel (JCPDS card no. 35-0782, space group:  $Fd3m$ ) undisputedly, indicating the high purity of the products. Diffraction peak of LLTO presents clearly in LLT05 samples. Absent diffraction peaks of LLTO in LLT01 and LLT03 samples is possible because the contents of LLTO are low to be detected. The coated samples do not show significant change in the lattice parameter. Lattice parameters of pristine  $\text{LiMn}_2\text{O}_4$  and LMO@LLTO are calculated by Jade 5.0 and shown in Table S1 (see ESI). It is clear the lattice parameters of  $\text{LiMn}_2\text{O}_4$  have no obvious variation, indicating main spinel structure remains unchanged after surface

modification. Furthermore, radius of  $\text{Mn}^{3+}$  (0.066 nm) and  $\text{Mn}^{4+}$  (0.060 nm) is much smaller than that of  $\text{La}^{3+}$  (0.106 nm), it can be inferred that if manganese ions were substituted by  $\text{La}^{3+}$ , the lattice parameter of the treated sample would be obvious different from that of pristine  $\text{LiMn}_2\text{O}_4$ . Therefore, it demonstrates that the LLTO layer on the surface of spinel  $\text{LiMn}_2\text{O}_4$ , rather than incorporated into the host structure. In order to obtain the information of LLTO and LMO@LLTO composites particle size distribution, particles are measured by laser particle size analyzer and the results are depicted in Fig. S2. The successful coating process can be ascribed to ball milling and effect of surfactant which can promote particle adhesion, because the melting carbon in high temperature can wrap in the outer surface of pellets and combust in much higher temperature during oxygen atmosphere.

To confirm LLTO coatings on the surface of  $\text{LiMn}_2\text{O}_4$  cathodes, XPS is employed to characterize the surface elements. The XPS spectra of Mn 2p, Ti 2p and La 3d for LLT0 and LLT01 are given in Fig. 2. Fig. 2a and Fig. 2b show the XPS spectra for Mn 2p of LLT0 and LLT01, respectively. The Two main peaks, which can be decomposed into two components ( $\text{Mn}2p_{3/2}$  and  $\text{Mn}2p_{1/2}$ ), are observed in the spectra for the  $\text{LiMn}_2\text{O}_4$ .<sup>45</sup> As shown in Fig. 2a, the observed binding energy values for  $\text{Mn}^{3+}$  are 652.9 eV ( $\text{Mn}2p_{1/2}$ ) and 640.7 eV ( $\text{Mn}2p_{3/2}$ ), while those of  $\text{Mn}^{4+}$  are 654.1 eV ( $\text{Mn}2p_{1/2}$ ) and 641.8 eV ( $\text{Mn}2p_{3/2}$ ). For sample LLT01, there are no obvious peak shifts in binding energy values with LLTO coating, which indicates the manganese oxidation state in the two samples are same. The XPS spectra of La3d and Ti2p are given in Fig. 2c. This figure shows La3d peaks at binding energy of 836.9 eV and

833.0eV, which can be conformed to the La-O chemical bond of  $\text{La}_2\text{O}_3$  in reference to the values in NIST XPS Database. As Fig. 2d displays, the Ti2p peaks around 463.6 eV, 461.4 eV and 456.3 eV correspond to  $\text{Ti}^{4+}(2p_{1/2})$ ,  $\text{Ti}^{3+}(2p_{1/2})$  and  $\text{Ti}^{3+}(2p_{3/2})$ .<sup>46</sup> These conclusions confirm the presence of LLTO coating on  $\text{LiMn}_2\text{O}_4$  cathode, which can be observed to mutually agree with analysis results of XRD.

Fig. 3 shows the morphologies of LLT0, LLT01, LLT03, LLT05 samples, respectively. It is clearly observed that pristine  $\text{LiMn}_2\text{O}_4$  present a smooth, angular, and no fragment surface. While after modification, the surface becomes coarse and particles of LLTO-coated samples are more aggregate with increasing weight ratio of LLTO. The morphologies and particle diameters of pristine  $\text{LiMn}_2\text{O}_4$  (Fig. 3a) are similar to LLT01 (Fig. 3b) in large field of view. The reason for this phenomenon may be LLTO coating content is too lower to be observed. In comparison, obscure particle surfaces and edges are exhibited in Fig. 3(c-d), and more fragments appear on the particle surface or among the particles with increasing LLTO coating contents. EDS measurement is also performed for LLT01 sample, and the images are shown in Fig. 3e. Lanthanum and titanium can be clearly observed on the surface of the sample. These results indicate that the LLTO are successfully coated on the surface of  $\text{LiMn}_2\text{O}_4$ .

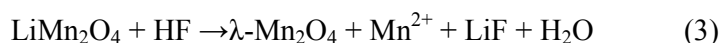
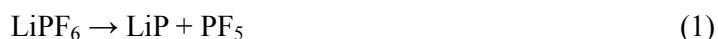
All the morphological and structural characteristics details of  $\text{LMO@LLTO}$  are further characterized by transmission electron microscopy (TEM). The typical TEM and high resolution TEM (HRTEM) images of LLT0 and LLT01 are shown in Fig. 4, with the inset showing selected-area electron diffraction pattern (SAED). The low

magnification TEM micrograph indicates pristine  $\text{LiMn}_2\text{O}_4$  particles have a smooth surface and without any attached particles (Fig. 4a). While Fig. 4b shows that  $\text{LiMn}_2\text{O}_4$  is well covered by a thin LLTO layer roughly 15-20 nm. As shown in Fig. 4c, lattice fringe with width of 0.48 nm corresponds to the (111) plane. Also the diffraction spots, which are uniformly indexed to the planes of (311) and (400) of face-centered cubic  $\text{LiMn}_2\text{O}_4$  structure, reveal highly crystalline phase. The LLTO layer is crystalline, with lattice fringes extending to the grain boundary (Fig. 4d). Only one diffraction fringe with lattice distance of 0.25 nm, corresponding to the d-spacing of the (110). The LLTO layers of the samples exhibit similar spotted patterns. It is likely that the LLTO diffuse into the surface and react with elements of the bare material such as Li and Mn due to high surface free energy of nanoparticles.<sup>47</sup>

The initial, 50<sup>th</sup>, 100<sup>th</sup> and 200<sup>th</sup> discharge curves of LLT0 and LLT01 cycled at 1 C at 25 °C and 55 °C are shown in Fig. 5. It can be seen that all discharge curves exhibited two plateaus at about 4.1 and 4.0 V vs.  $\text{Li/Li}^+$ , corresponding to two-step process during cycling.<sup>48</sup> As presented in Fig. 5a, LLT0 electrode delivered a relatively high discharge capacity of 124  $\text{mAh g}^{-1}$ , while LLT01 showed a slightly lower capacity of 117  $\text{mAh g}^{-1}$ . However, LLT0 suffers remarkable capacity fading during subsequently cycles. As we intended, the amount of LLTO layer is approximate 1 wt% in these LMO@LLTO cathode materials. This concern can be confirmed by comparing the capacities as shown in Fig. 5a and the ESI, Fig. S3. Similar results can be found in Fig. 5b. It should be noted that 4.1 V platform of LLT01 sample shows slightly higher than that of LLT0 at 55 °C. We consider LLTO

layer benefits to reduce impedance of Li<sup>+</sup> diffusion and suppress HF-induced Mn dissolution at elevated temperature.

The cycle performance and rate capability of the samples tested at 25 °C and 55 °C are shown in Fig. 6. Fig. 6a shows the cycling performances of the LLT0, LLT01, LLT03 and LLT05 at a current density of 1 C in the voltage range of 3.0-4.3V. The beneficial effect of LLTO-coating on enhancing cycling performances can be observed obviously. Although discharge capacity of pristine LiMn<sub>2</sub>O<sub>4</sub> is larger than that of coated samples during initial cycle, the capacity retention rates of LLT0, LLT01, LLT03 and LLT05 after 200 cycles are 78.6 %, 90.8 %, 83.9 % and 77.8 %, respectively. It demonstrates LLTO-coated LiMn<sub>2</sub>O<sub>4</sub> are more stable in the repeated cycling, especially the LLT01 sample. We think that large amount of LLT coating will lead to more difficulty of electrolyte wetting process and few active materials. Considering reduced discharge capacity with increased coating amount, the optimized LLTO coating amount is 1 wt% upon our present study. In comparison, cycling efficiency of LLT0 is lower than that of the other three samples. This capacity fade could be a result of side reactions with electrolyte due to manganese ion. The side reactions are reported by previous literatures.<sup>9, 49-51</sup> It is suggest that HF generated from LiPF<sub>6</sub>-based electrolyte is responsible for Mn dissolution during cycling, and the chemical equations as shown below:<sup>52</sup>



These reactions indicate the acid is self-catalytic, and HF is regenerated by the reaction of water with  $\text{LiPF}_6$ . At the same time, HF attacks the surface of cathode, and thus the Mn ions in the structure of the cathode dissolve into the electrolyte. Furthermore, water produced from equation (3) will promote the equation (2) which leads to quicken up Mn dissolution. However, the LLTO layer can effectively reduce direct contact between  $\text{LiMn}_2\text{O}_4$  and electrolyte, thus decrease dissolution of Mn ions, resulting in coated  $\text{LiMn}_2\text{O}_4$  with better cycle performance than that of pristine  $\text{LiMn}_2\text{O}_4$ . Cyclic performances of LLT0 and LLT01 samples at 55 °C are also evaluated (Fig. 6b). Before electrochemical testing, cells are put in an incubator chamber at 55 °C for 5 days, where it is monitored regularly. As for LLT0 sample, discharge capacity fades to 82 mAh  $\text{g}^{-1}$  at the 200<sup>th</sup> cycle with a capacity retention ratio of 70.8 %. In contrast, the LLT01 sample still shows 90.4 % capacity retention after 200 cycles. The improved cycle performance of coated electrode probably result from the existence of solid electrolyte LLTO layer which can effectively protect the  $\text{LiMn}_2\text{O}_4$  particles from direct contact with the electrolyte during the long-term cycling.

The rate capability highlights advantage of LLTO coatings are shown in Fig. 6c-d. We can find that cycle performance of LLT0 suffers fast fading in different rates, though it exhibits a higher discharge capacity at 0.5 C. What is more, at higher rates, values for pristine  $\text{LiMn}_2\text{O}_4$  are much lower than those of coated samples. For instance, LLT01 deliver 87 mAh  $\text{g}^{-1}$  on average discharge at 5 C (75.4% of initial discharge capacity at 0.5 C), while that of the pristine electrode is 77 mAh  $\text{g}^{-1}$  (66.5%).

The results indicate LLTO layer acts as a high lithium ion conductor and clear channel for Li ion diffusion. Discharge capacity of LLT01 and LLT0 can be recovered to 112 mAh g<sup>-1</sup> and 100 mAh g<sup>-1</sup> at 0.5 C, which with a retention of 81 % and 70 % of initial discharge capacity, respectively. This demonstrates LLT01 electrode has better electrochemical reversibility and structural stability than that of LLT0. According to Fig. 6d, both of the samples exhibit similar initial discharge capacity at lower C-rate (0.5 C). However, the data reveal LLT01 delivers obviously higher discharge capacity compared to LLT0 at high C-rate. For example, LLT01 retains 85 % of its full discharge capacity while LLT0 only retains 60% at 5C rate, which indicating excellent rate capability of LMO@LLTO.

To obtain a better understanding of the advantageous effect of LLTO coating layer on the rate and cycle performances, CV studies were taken at a scan rate of 0.1 mV s<sup>-1</sup> at room temperature. Fig. 7a shows the second and fiftieth CV curves of LLT01 and LLT0 samples, respectively. The CV curves of both LiMn<sub>2</sub>O<sub>4</sub> and LMO@LLTO electrodes reveal two sharp pairs of redox peaks, suggesting that lithium ions are extracted and inserted from/into the spinel phase by a two-step process. The pair of redox peaks at 4.09/3.96 V corresponds to insertion of Li<sup>+</sup> into half of tetrahedral sites with Li-Li interaction. And the pair of redox peaks at 4.19/4.07 V correspond to extraction of Li<sup>+</sup> from half of tetrahedral sites without Li-Li interaction.<sup>53</sup> In comparison with the CV curves, LMO@LLTO shows two high pairs of distinct oxidation current peaks and reduction current peaks, demonstrating the occurrence of lower polarization and reversible oxidation reaction process. Furthermore,

high-symmetric redox peaks are still retained even after 50 cycles at 1 C rate. But for the pristine  $\text{LiMn}_2\text{O}_4$ , clear reduction of peak current densities can be found. This can be ascribed to the separation effect between electrolyte and active material, restraining manganese dissolution and improving reversibility of  $\text{Li}^+$  transport at the interface. Usually, electrochemical reaction of the batteries follows three steps:  $\text{Li}^+$  diffusion inside the electrode materials, charge transfer reaction at the interface between the electrode and electrolyte, and  $\text{Li}^+$  movement in the electrolyte. As shown in Fig. 7b, the LLTO lithium superionic conductor layer reduced the charge transfer reaction at the interface thus improving total  $\text{Li}^+$  ionic conductivity. This could be observed to mutually agree with fitting values for LLT0 and LLT01 during initial discharge-charge cycle by EIS.

To explore changes of electrode/electrolyte interface during cycle, EIS measurements are taken at room temperature on the cells during the initial discharge-charge cycle. The data are collected at various voltages in the potential range from 4.2 to 3.0 V at 0.5 C. Since the stable cycle performance, EIS are carried out only on LLT01 sample. For comparison, EIS of LLT0 are also conducted. For the best view, Fig. 8a-d shows partial enlarge of three-dimensional Nyquist plots for the initial discharge-charge cycle. Details of the whole plots are shown in Fig. S4. The original data are fitted using two equivalent circuit models (Fig. 8e). The kinetic parameters are obtained by simulation, including resistance of the electrolyte ( $R_s$ ), surface film capacitance ( $CPE_{sf}$ ) and resistance for  $\text{Li}^+$  migration through the surface film ( $R_f$ ), charge-transfer resistance at the bulk-electrolyte interface ( $R_{ct}$ ), double-layer

capacitance ( $CPE_{dl}$ ).<sup>54, 55</sup> The inclined line in the low frequency range corresponding to the Warburg impedance ( $Z_w$ ). Generally, the semicircle of impedance spectra at the high frequency range is related to diffusion resistance of  $Li^+$  ions through the solid-electrolyte interphase (SEI) layer. The semicircle in the medium-frequency range indicates the charge transfer resistance.<sup>56, 57</sup> The diffusion coefficient of  $Li^+$  ions ( $D_{Li^+}$ ) can be calculated by the method described in Table S2.

From Fig. 8, it can be seen that the semicircle of LLT01 is smaller than that of LLT0. According to the impedance values (Table S2), the fitting result of the initial charge transfer resistance of LLT0 is 110.8  $\Omega$  at open circuit voltage (OCV). Whereas, the LLT01 electrode has a  $R_{ct}$  value of 37.69  $\Omega$ , which was almost one-third of the LLT0. During the discharge process, the value of  $R_{ct}$  decreases with an increase in potential (Fig. 8b and Fig. 8d). A higher potential would be helpful to  $Li^+$  insertion into the lattice. This is in accordance with results reported by Dokko et al.<sup>58</sup> The variation of  $D_{Li^+}$  with potential are shown in Table S2.  $D_{Li^+}$  varies within  $10^{-11}$  to  $10^{-13}$   $cm^2 s^{-1}$ , which is closest to reported by Lu et al and Zhao et al.<sup>59, 60</sup> The value of  $D_{Li^+}$  decreases with increasing potentials. This phenomenon indicates that the amount of inserted  $Li^+$  has effects on diffusion process of  $Li^+$ . This is in good agreement with the results obtained by electrochemical properties test at 25 °C. Based on the EIS results, it appears that the LLTO coating layer can suppress increase of charge transfer resistance and keep a relatively smooth passage for lithium ion diffusion on  $LiMn_2O_4$  particle surface.

$LiMn_2O_4$  shows severe capacity fading at elevated temperature. This is mainly

affected by Mn dissolution in HF-containing electrolyte.<sup>50</sup> Therefore, it is necessary to address the effect of LLTO coating on Mn dissolution. Thus, ICP is employed to analysis the concentration of the Mn in the electrolytes after different cycles at elevated temperature. As Table 1 displays, Mn content in the electrolyte for LLT0 is of magnitude more than that for LL01. This indicates that the LLTO coating layer effectively suppress Mn loss into the electrolyte. Electronic conductivity of the cathode is also a key issue to determine the electrochemical performance of the battery. LLT01 shows higher electronic conductivity than that of LLT0, indicating that LLTO coating improve electronic conductivity of  $\text{LiMn}_2\text{O}_4$ . This is in consistent with the results of rate performance (Table S3).

#### 4. Conclusions

In summary, by exploiting liquid-phase coating and calcination procedures, we have successfully designed and synthesized core-shell  $\text{LMO@LLTO}$  cathode materials that have unique properties in terms of rate capability and cycling stability. It exhibits a high discharge capacity of  $111 \text{ mAh g}^{-1}$  at 1 C and still 90.4 % capacity retention after 200 cycles even at  $55 \text{ }^\circ\text{C}$  high temperature. The great improvement for rate and cycle performance could be attributed to high ionic conductivity and controllable Mn dissolution from LLTO layer. The results herein support the idea  $\text{LMO@LLTO}$  could be a competitive candidate cathode material for high-performance LIB used for HEVs or EVs. Owing to superior properties of this structure, we expect it will be widely used in designing other electrode materials for enhancing the rate and cycling capability of batteries.

## Acknowledgements

This research was supported by the National Natural Science Foundation of China (51364004), Guangxi Natural Science Foundation (2013GXNSFDA019027), Science and Technology Research Program of Young Talent Project of Hubei Provincial Department of Education (Q20142901), Hubei Province Undergraduate Training Programs for Innovation and Entrepreneurship (201310514017) and Shenzhen Basic Research Project (JCYJ20120619140233056).

## References

- 1 J. B. Goodenough, K. S. Park. *J. Am. Chem. Soc.* 2013, 135, 1167-1176.
- 2 M. Hu, X. Pang, Z. Zhou. *J. Power Sources.* 2013, 237, 229-242.
- 3 M. Armand, J.M. Tarascon. *Nature.* 2008, 451, 652-657.
- 4 J. Lee, A. Urban, X. Li, D. Su, G. Hautier, G. Ceder. *Science*, 2014, 343, 519-522.
- 5 J. K. Noh, S. Kim, H. Kim, W. Choi, W. Chang, D. Byun, B. W. Cho, K. Y. Chung. *Sci. Rep.* 2014, 4, 4847.
- 6 S. Afyon, M. Wörle, R. Nesper. *Angew. Chem. Int. Ed.* 2013, 52, 12541-12544.
- 7 M. J. Lee, S. Lee, P. Oh, Y. Kim, J. Cho. *Nano Lett.* 2014, 14, 993-999.
- 8 Y. Qiao, S. R. Li, Y. Yu, C. H. Chen. *J. Mater. Chem. A.* 2013, 1, 860-867.
- 9 H. Zhuo, S. Wan, C. He, Q. Zhang, C. Li, D. Gui, C. Zhu, H. Niu, J. Liu. *J. Power Sources.* 2014, 247, 721-728.
- 10 S. Lee, Y. Oshima, E. Hosono, H. Zhou, K. Kim, H. M. Chang, R. Kanno, K. Takayanagi. *J. Phys. Chem. C.* 2013, 117, 24236-24241.
- 11 M. V. Reddy, G. V. Subba Rao, B. V. R. Chowdari. *Chem. Rev.* 2013, 113,

5364-5457.

- 12 O. K. Park, Y. Cho, S. Lee, H. C. Yoo, H. K. Song, J. Cho. *Energy Environ. Sci.* 2011, 4, 1621-1663.
- 13 A. Yamada, M. Tanaka. *Mater. Res. Bull.* 1995, 30, 715-721.
- 14 K. Y. Chung, K. B. Kim. *Electrochim. Acta.* 2004, 49, 3327-3337.
- 15 K. Kuriyama, A. Onoue, Y. Yuasa, K. Kushida. *Surf. Sci.* 2007, 601, 2256-2259.
- 16 Y. Terada, Y. Nishiwaki, I. Nakai, F. Nishikawa. *J. Power Sources.* 2001, 97-98, 420-422.
- 17 H. Zhang, Y. Xu, D. Liu, X. Zhang, C. Zhao. *Electrochim. Acta.* 2014, 125, 225-231.
- 18 M. V. Reddy, A. Sakunthala, S. SelvashekaraPandian, B.V.R. Chowdari, Preparation. *J. Phys. Chem. C.* 2013, 117, 9056-9064.
- 19 M. V. Reddy, S. Sundar Manoharan, J. John, B. Singh, G. V. Subba Rao, B.V.R. Chowdari. *J. Electrochem. Soc.* 2009, 156, A652-A660.
- 20 H. Zhang, Y. Xu, D. Liu, X. Zhang, C. Zhao. *Electrochim. Acta.* 2014, 125, 225-231.
- 21 Y. Shin, A. Manthiram. *J. Electrochem. Soc.* 2004, 151, A204-A208.
- 22 X. Li, J. Liu, X. Meng, Y. Tang, M.N. Banis, J. Yang, Y. Hu, R. Li, M. Cai, X. Sun. *J. Power Sources*, 247, 2014, 57-69.
- 23 D. Guan, J. A. Jeevarajan, Y. Wang. *Nanoscale.* 2011, 3, 1465-1469.
- 24 J. S. Gnanaraj, V. G. Pol, A. Gedanken, D. Aurbach. *Electrochem. Commun.* 2003, 5, 940-945.
- 25 S. J. Shi, J. P. Tu, Y. Y. Tang, X. Y. Liu, Y. Q. Zhang, X. L. Wang, C. D. Gu.

- Electrochim. Acta.* 2013, 88, 671-679.
- 26 J. Zhao, Y. Wang. *Nano Energy.* 2013, 2, 882-889.
- 27 K. A. Walz, C. S. Johnson, J. Genthe, L. C. Stoiber, W. A. Zeltner, M. A. Anderson, M. M. Thackeray. *J. Power Sources.* 2010, 195, 4943-4951.
- 28 H. Liu, C. Cheng, Z. Hu, K. Zhang. *Mater. Chem. Phys.* 2007, 101, 276-279.
- 29 J. Tu, X. B. Zhao, J. Xie, G. S. Cao, D. G. Zhuang, T. J. Zhu, J. P. Tu. *J. Alloy. Compd.* 2007, 432, 313-317.
- 30 L. Feng, S. Wang, L. Han, X. Qin, H. Wei, Y. Yang. *Mater. Lett.* 2012, 78, 116-119.
- 31 D. Arumugam, G. Paruthimal Kalaignan. *Mater. Res. Bull.* 2010, 45, 1825-1831.
- 32 X. Li, Y. Xu. *Appl. Surf. Sci.* 2007, 253, 8592-8596.
- 33 M. Michalska, B. Hamankiewicz, D. Ziółkowski, M. Krajewski, L. Lipińska, M. Andrzejczuke, A. Czerwiński. *Electrochim. Acta.* 2014, 136, 286-291.
- 34 J.H. Lee, K.J. Kim. *Electrochim. Acta.* 2013, 102, 196-201.
- 35 H. Ming, Y. Yan, J. Ming, J. Adkins, X. Li, Q. Zhou, J. Zheng. *Electrochim. Acta.* 2014, 120, 390-397.
- 36 S. J. Shi, J. P. Tu, Y. J. Mai, Y. Q. Zhang, C. D. Gu, X. L. Wang. *Electrochim. Acta.* 2012, 63, 112-117.
- 37 S. Zhao, Y. Bai, Q. Chang, Y. Yang, W. Zhang. *Electrochim. Acta.* 2013, 108, 727-735.
- 38 K. S. Tan, M. V. Reddy, G. V. Subba Rao, B.V.R. Chowdari. *J. Power Sources.* 2005, 141, 129-142.
- 39 X. Wu, X. Li, Z. Wang, H. Guo, L. Xiong. *Ionics.* 2012, 18, 907-911.

- 40 X. Li, J. Liu, M.N. Banis, A. Lushington, R. Li, M. Cai, X. Sun. *Energy Environ. Sci.* 2014, 7, 768-778.
- 41 Y. Inaguma, C. Liqun, M. Itoh, T. Nakamura, T. Uchida, H. Ikuta, M. Wakihara. *Solid State Commun.* 1993, 86, 689-693.
- 42 M. Prabu, M. V. Reddy, S. Selvasekarapandian, S. Admas, K. P. Loh, G.V.S. Rao, B.V.R. Chowdari. *J. Electrochem. Soc.* 2013, 160, A3144-A3147.
- 43 S. X. Zhao, X. F. Fan, Y. F. Deng, C. W. Nan. *Electrochim. Acta.* 2012, 65, 7-12.
- 44 S. Noh, J. Kim, M. Eom, D. Shin. *Ceram. Int.* 2013, 39, 8453-8458.
- 45 M. C. Biesinger, B. P. Payne, A. P. Grosvenor, L. W. M. Lau, A. R. Gerson, R. A. Smart. *Appl. Surf. Sci.* 2011, 257, 2717-2730.
- 46 M. K. Rath, B. G. Ah, B. H. Choi, M. J. Ji, K. T. Lee. *Ceram. Int.* 2013, 39, 6343-6353.
- 47 H. J. Lee, K. S. Park, Y. J. Park. *J. Power Sources.* 2010, 195, 6122-6129.
- 48 M. Prabu, M. V. Reddy, S. Selvasekarapandian, G. V. Subba Rao, B.V.R. Chowdari. *Electrochim. Acta.* 2013, 88, 745-755.
- 49 S. T. Myung, K. Hosoya, S. Komaba, H. Yashiro, Y. K. Sun, N. Kumagai. *Electrochim. Acta.* 2006, 51, 5912-5919.
- 50 D. Aurbach. *J. Power Sources.* 2000, 89, 206-218.
- 51 D. H. Jang, Y. J. Shin, S. M. Oh. *J. Electrochem. Soc.* 1996, 143, 2204-2211.
- 52 K. T. Lee, S. Jeong, J. Cho. *Accounts Chem. Res.* 2012, 46, 1161-1170.
- 53 M. M. Thackeray, W. I. F. David, P. G. Bruce, J. B. Goodenough. *Mat. Res. Bull.* 1983, 18, 461-472.

- 54 Q. Chen, Y. Wang, T. Zhang, W. Yin, J. Yang, X. Wang. *Electrochim. Acta.* 2012, 83, 65-72.
- 55 J. Liu, A. Manthiram. *J. Phys. Chem. C.* 2009, 113, 15073-15079.
- 56 Y. Wu, Z. Wen, H. Feng, J. Li. *small.* 2012, 8, 858-862.
- 57 W. Liu, J. Liu, K. Chen, S. Ji, Y. Wan, Y. Zhou, D. Xue, P. Hodgson, Y. Li. *Chem. Eur. J.* 2014, 20, 824-830.
- 58 K. Dokko, M. Mohamedi, Y. Fujita, T. Itoh, M. Nishizawa, M. Umeda, I. Uchida. *J. Electrochem. Soc.* 2001, 148, A422-A426.
- 59 D. Lu, W. Li, X. Zuo, Z. Yuan, Q. Huang. *J. Phys. Chem. C.* 2007, 111, 12067-12074.
- 60 X. Zhao, M. V. Reddy, H. Liu, S. Ramakrishna, G. V. Subba Rao, B. V. R. Chowdari. *RSC Adv.* 2012, 2, 7462-7469.

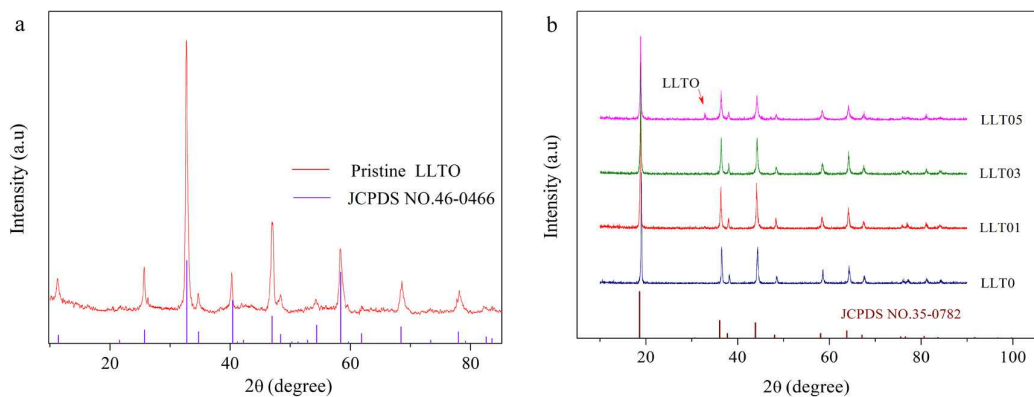


**Fig. 1.** XRD patterns of (a) pristine LLTO and (b) LLT0, LLT01, LLT03, LLT05 samples.

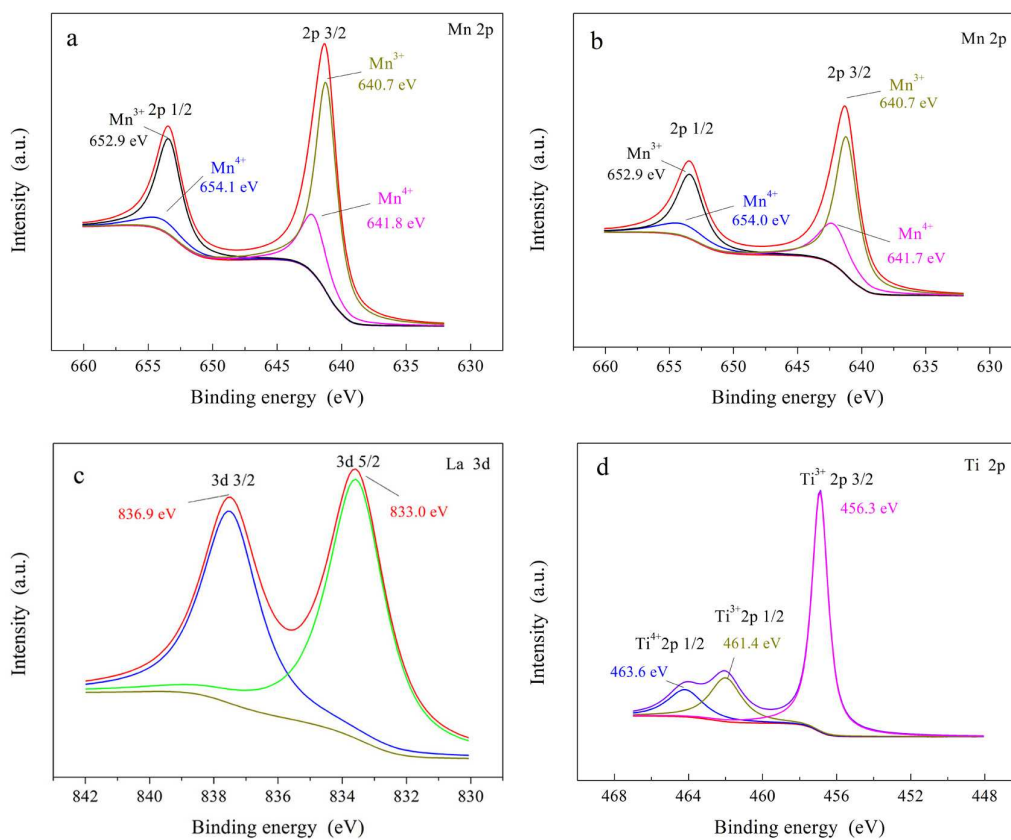


**Fig. 2** The XPS patterns of the LLT0 and LLT01 a) Mn 2p spectra for LLT0; b) Mn 2p spectra for LLT01; c) La 3d spectra for LLT01; d) Ti 2p spectra for LLT01

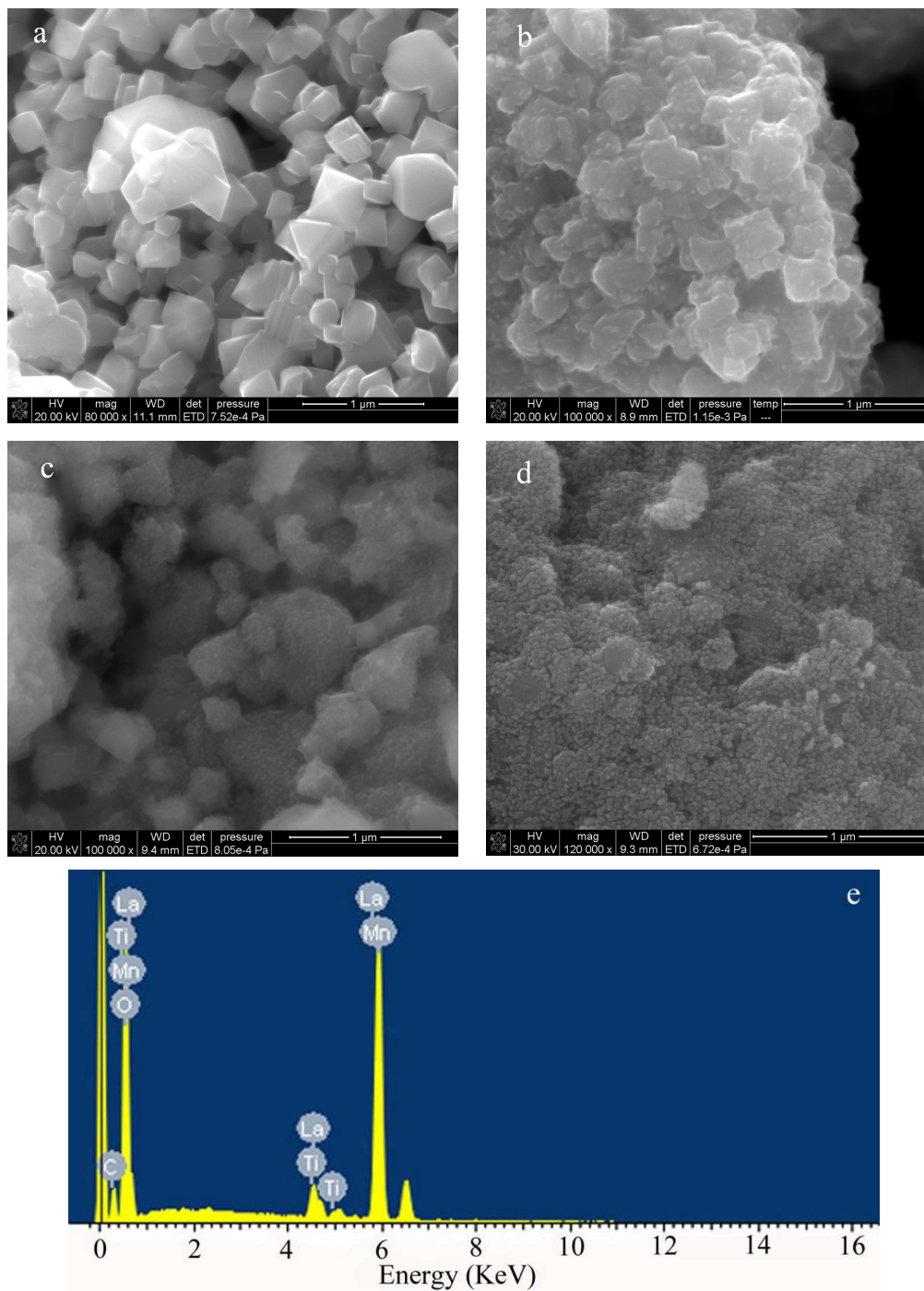


**Fig. 3.** SEM images of pristine (a) LLT0, (b) LLT01, (c) LLT03, (d) LLT05 and the EDS mappings of LLT01 (e).

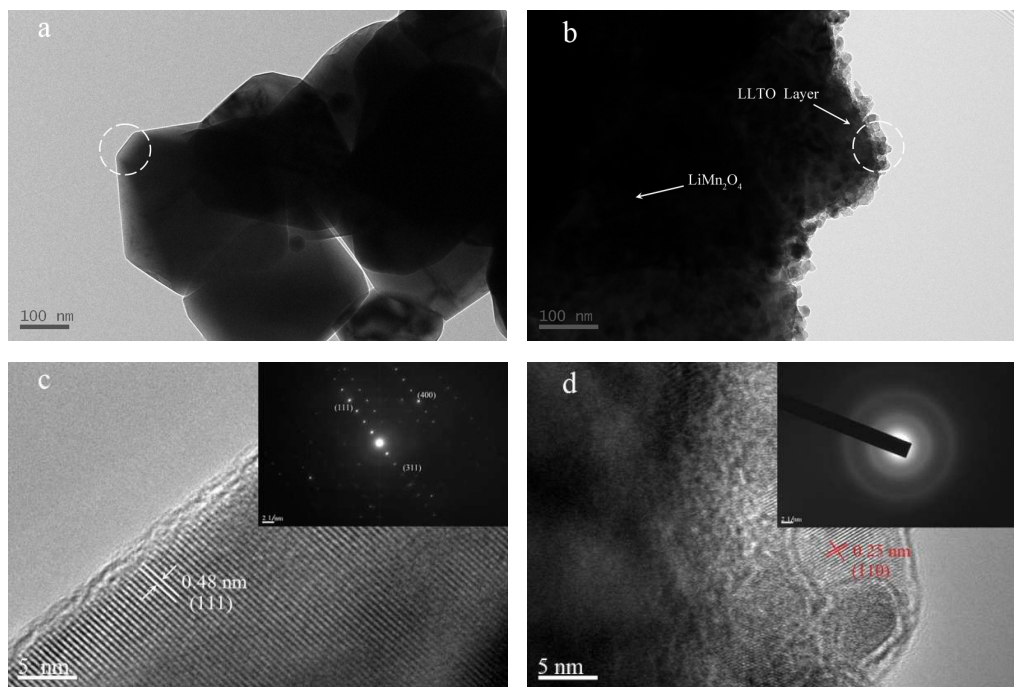


**Fig. 4.** TEM (a, b) and HRTEM (c, d) images of LLTO and LLTO1 (the inset shows corresponding SAED pattern), respectively.

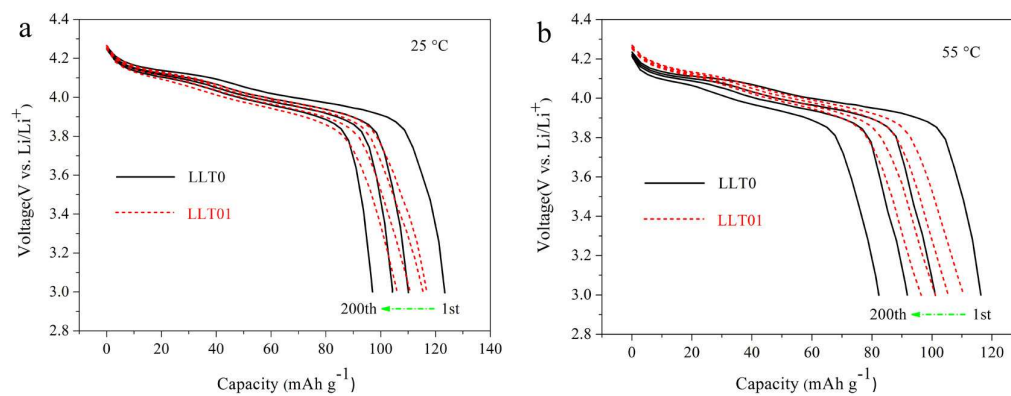


**Fig. 5.** The initial, 50<sup>th</sup>, 100<sup>th</sup> and 200<sup>th</sup> discharge curves of LLTO and LLTO1 cycled at 1 C at 25 °C (a) and 55 °C (b).

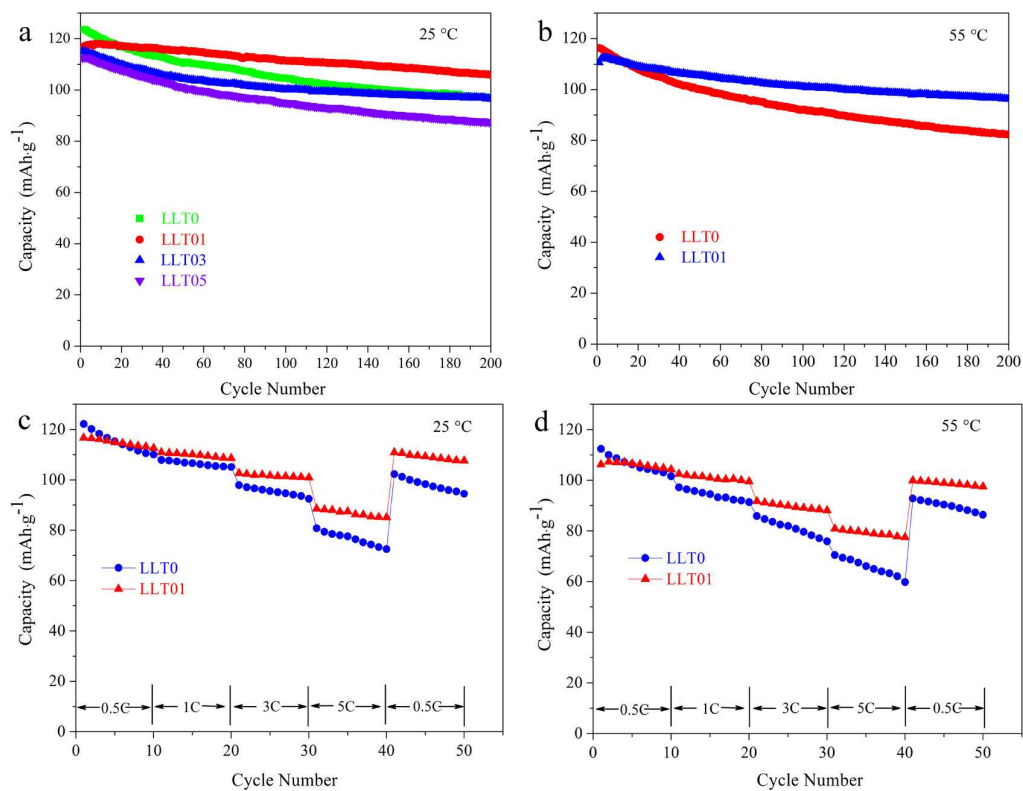


**Fig. 6.** (a, b) Cycling performance of the samples at the rate of 1 C and (c, d) plots of discharge capacity values of the samples at different rates from 0.5 C to 5 C in the voltage range of 3.0-4.3V at 25 °C and 55 °C.

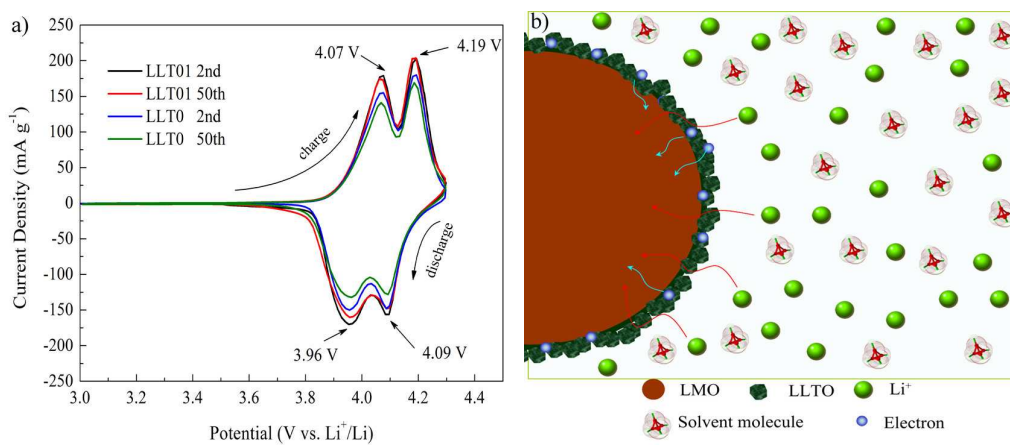


**Fig. 7** a) CV curves of LLT0 and LLT01 cathode at a scan rate of 0.1 mV s<sup>-1</sup> after different cycles at 1 C rate at room temperature; b) Scheme illustration of LLTO surface coating for the LMO cathode material.

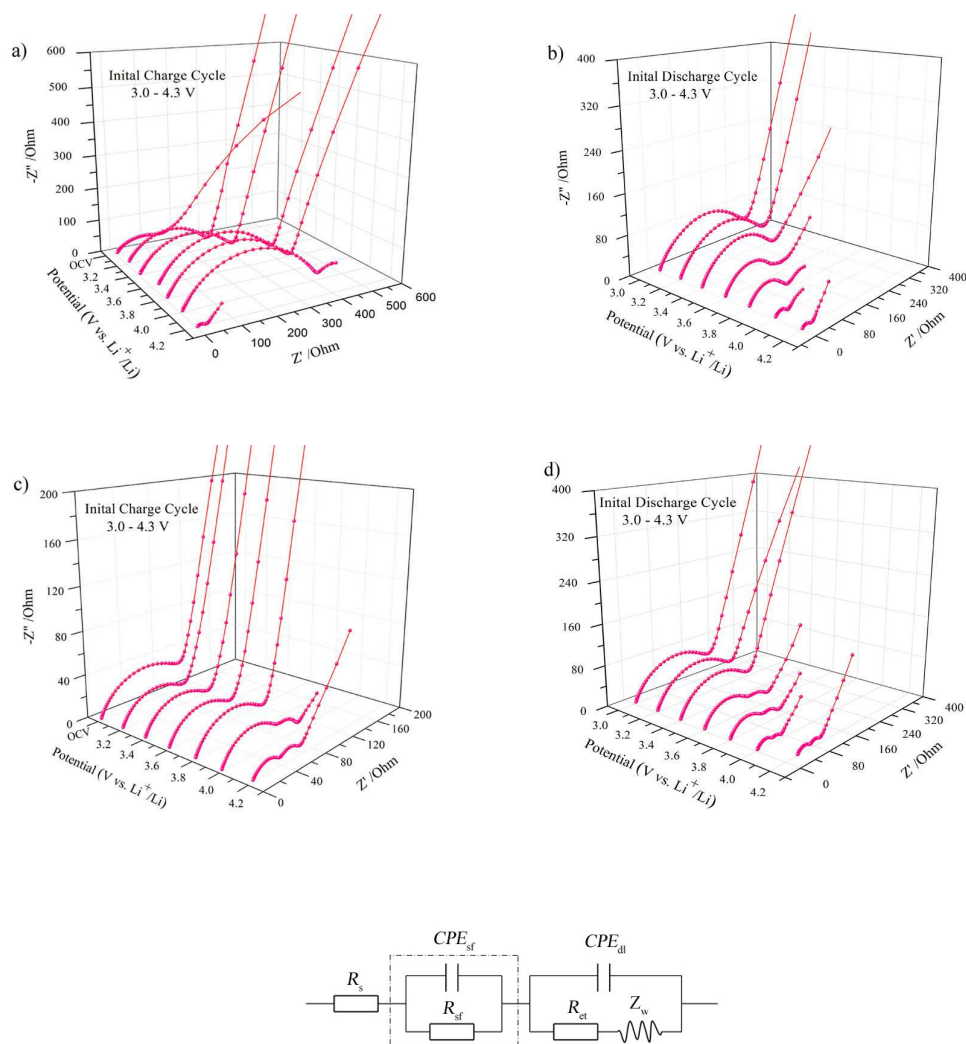


**Fig. 8.** Partial enlarge of the three-dimensional Nyquist plots for LLT0 (a) initial charge cycle (3.2-4.2 V), (b) initial discharge cycle (4.2-3.0 V) and LLT01 (c) initial charge cycle (3.2-4.2 V), (d) initial discharge cycle (4.2-3.0 V). (e) Equivalent circuit used for fitting the impedance spectra consisting of  $R_s$  and  $R_{ct}/CPE_{dl}$  combinations ( $R_f$  and  $CPE_{sf}$  are included only for the spectra corresponding to some potential).

**Table 1.** ICP analyses results of Mn contents in the electrolyte of LLT0 and LLT01 after different cycles at 55 °C

Cycle numbers		50	100	200
Mn content in the electrolyte (ppm)	LLT0	3.2	5.5	8.7
	LLT01	0.24	0.45	0.66

